J Mater Sci (2012) 47:2264–2270
DOI 10.1007/s10853-011-6038-y

Microwave adsorption of core–shell structured $Sr(MnTi)_xFe_{12-2x}O_{19}$/PANI composites

H. M. Kuo · Te-Fa Hsui · Y. S. Tuo · C. L. Yuan

Received: 2 August 2011 / Accepted: 7 October 2011 / Published online: 20 October 2011

Abstract Polyaniline polymer-coated MnTi-substituted strontium hexaferrite ($Sr(MnTi)_xFe_{12-2x}O_{19}$/PANI, $x = 1.0, 1.5, 2.0$) composites were synthesized by the oxidative chemical polymerization of aniline in the presence of ammonium peroxydisulfate. The structure and morphologies of the products were characterized by X-ray diffraction, FT-IR, TGA, SEM, and TEM. In the magnetization for the $Sr(MnTi)_xFe_{12-2x}O_{19}$/PANI composites, it was found that the saturation magnetization (M_s) and coercivity (H_c) decreased after polyaniline coating. The composite under an applied magnetic field exhibited hysteretic loops of ferromagnetic behavior, such as high saturation magnetization ($M_s = 12.1$–1.9 emu/g) and coercivity ($H_c = 0.919$–0.084 kG). The composite specimens of core–shell $Sr(MnTi)_xFe_{12-2x}O_{19}$/PANI and thermal plastic resin had a band-width microwave absorption due to the reflection losses from −15 to −35 dB at frequencies between 18 and 40 GHz as observed by a high-frequency network analyzer.

H. M. Kuo
Department of Mitochondrial Research Unit, Chang Gung Memorial Hospital-Kaohsiung Medical Center, Chang Gung University College of Medicine, Kaohsiung, Taiwan

T.-F. Hsui
Department of Cosmetic Applications & Management, Tung Fang Institute of Technology, Kaohsiung, Taiwan

Y. S. Tuo
Department of Chemical and Materials Engineering Chung Cheng Institute of Technology, National Defense University, Taoyuan, Taiwan

C. L. Yuan (✉)
Department of Chemistry, R. O. C. Military Academy, Fengshan, Kaohsiung, Taiwan
e-mail: junelong@mail2000.com.tw

Introduction

M-type hexaferrites have a large intrinsic magnetic anisotropy field, and the variation of this field is caused by Sr^{2+} and Fe^{3+} ions being substituted by extrinsic metallic ions. As a result, the applications of M-type hexaferrites in both microwave resonant and microwave non-resonant devices are very important [1]. Such types of M-type hexaferrites have also continued to be of great interest for both the applications of microwave absorbers and the protectoral materials of electromagnetic interference (EMI) on electronic and communication equipment [2, 3]. The M-type hexaferrites are advantageous because of their high permeability and high resonant frequency. $Ba(MnTi)_{1.6}Fe_{8.8}O_{19}$ shows a strong microwave absorption within the frequency range of 8.0–12.0 GHz [4].

Many different methods of producing ferrites have been developed thus far. Such methods include, the dry method, the hydrothermal reaction [5–7], chemical co-precipitation [8–11], aerosol pyrolysis [12], the sol–gel technique [13–16], the glass crystallization method [7, 17, 18], low temperature combustion synthesis (LCS) [19, 20], and aqueous combustion synthesis (ACS) [21–23]. An ideal method to make hexaferrites should include a facile operation and low calcination temperature, and it should be energy-efficient and have a short reaction time. In addition, ultra-fine powder particles with narrow particle size distribution, excellent chemical homogeneity, and single magnetic domain are all required for ideal strontium M-type hexaferrite (Sr-M) resulting powders. The LCS method was used to synthesize $Ba(MnTi)_xFe_{12-2x}O_{19}$ hexaferrites [24]. The ACS method has not only the advantages described above but also the benefit that the wet sol–gels containing the proper amount of H_2O can be ignited directly and the thermal explosion

self-propagating combustion will be completed in a short time. The particle size distribution of the as-burnt powder was found to be between 30 and 50 nm; therefore, the ACS method was used for the preparation of Sr-M hexaferrites in the research presented here.

Conductive polyaniline has attracted much attention because of its potential applications in various fields, such as molecular electronics, chemical sensor, EMI shielding, antistatic coatings, rechargeable batteries, corrosion inhibitors, and microwave absorbing materials [25–29]. It is well known that conducting polymers can effectively shield electromagnetic waves generated by an electric source, whereas electromagnetic waves from a magnetic source can be effectively shielded only by magnetic materials [30, 31]. Thus, incorporation of magnetic constituents and conducting polymeric materials opens new possibilities for the achieving good shielding for various electromagnetic sources.

Until now, many reports have focused on selecting the hexaferrite as the magnetic component in polyaniline-based composites; see, e.g., [32–34]. Additionally, our laboratory has previously described a successful PANI/$SrFe_{12}O_{19}$ and $Sr(ZnZr)_xFe_{12-2x}O_{19}$/PANI synthesis using the chemical polymerization method [35, 36]. To our knowledge, there are no other existing reports on studies related to modifying the magnetic properties of conducting polyaniline coating and strontium manganese titanium hexaferrites composites ($Sr(MnTi)_xFe_{12-2x}O_{19}$/PANI) with our method.

In this study, electromagnetic functionalized $Sr(MnTi)_xFe_{12-2x}O_{19}$/PANI composites were synthesized by the oxidative chemical polymerization of aniline in the presence of ammonium peroxydisulfate (APS). The $Sr(MnTi)_xFe_{12-2x}O_{19}$ particles were the magnetic cores obtained using the ACS method in the glycine–metal nitrate sol–gel system, and polyaniline (PANI) was the conducting shell. The samples were characterized by various experimental techniques, and the magnetization properties of the composites were investigated. The absorption of microwaves and the *relatively* complex permittivity and permeability of the composite powders were also investigated.

Experimental

Materials

Aniline was distilled twice under reduced pressure and stored below 0 °C. Citric acid, ammonia, HCl, $Fe(NO_3)_3\cdot 9H_2O$, $Sr(NO_3)_2$, $Mn(NO_3)_2\cdot 6H_2O$, NH_2CH_2COOH, $Ti(NO_3)_4$, and $(NH_4)_2S_2O_8$ (APS) were all of analytical purity and used without further purification.

Preparation of $Sr(MnTi)_xFe_{12-2x}O_{19}$ hexaferrite particles

M-type hexaferrites of $Sr(MnTi)_xFe_{12-2x}O_{19}$, where $x = 0$, 1.0, 1.5, and 2.0, were synthesized using ACS in a glycine–metal nitrates system. The reaction equations of the ACS method for the preparation of hexaferrites and the formation of gaseous species [16] in these reactions can be described simply by the following:

$$\begin{aligned} &Sr(NO_3)_2 + xMn(NO_3)_2\cdot 6H_2O + xTi(NO_3)_4 \\ &\quad + (12-2x)Fe(NO_3)_3\cdot 9H_2O \\ &\quad + yNH_2CH_2COOH + zH_2O \xrightarrow[\text{evaporation}]{120\ ^\circ C} \text{wet sol-gels} \end{aligned} \quad (1)$$

$$\begin{aligned} &\text{Wet sol-gels} \xrightarrow[(2)\text{calcination}]{(1)\text{ignition}} Sr(MnTi)_xFe_{12-2x}O_{19} + mH_2O \\ &\quad + nCO_2 + pNO + qNH_3 \end{aligned} \quad (2)$$

The mole ratios of all starting metal nitrates in the reactions were controlled depending on the composition of the desired materials. We defined R as the molar ratio of glycine to the nitrate ions in the precursor solution. According to our experimental observation and the proposed ACS by Varma and coworkers [24], the value of R was fixed at 0.75 in all synthetic reactions to obtain the thermal explosion self-propagation combustion.

Using Eq. 3, the stoichiometric amount of metal nitrates were dissolved completely in 50 mL of deionized water to obtain aqueous solution I. Solution II was prepared by dissolving an appropriate amount of glycine into 50 mL of deionized water. Solutions I and II were further mixed to form a homogeneous transparent aqueous solution. Ammonium hydroxide (mass percent 28) was then added to the mixed solution to adjust the pH value. The mixed solutions were then heated in oil-bath at 120 °C for 1.5 h to evaporate approximately 50% of the water until high viscosity, wet sol–gels were formed. Finally, the wet sol–gels were ignited in an air atmosphere and the thermal explosion self-propagation combustion reactions were accomplished. The ash produced after combustion was deep reddish-brown and voluminous. The as-burnt powders were the precursors of M-type strontium hexaferrites. Furthermore, the M-type of cation-substituted strontium manganese titanium hexaferrites ($Sr(MnTi)_xFe_{12-2x}O_{19}$) were obtained after annealing the as-burnt powders at different temperatures for 2 h.

Polymerization of $Sr(MnTi)_xFe_{12-2x}O_{19}$/PANI composites

The core–shell structure materials of $Sr(MnTi)_xFe_{12-2x}O_{19}$/PANI, where $x = 0$, 1.0, 1.5, and 2.0, were prepared by

oxidative chemical polymerization of aniline on the surface of 10 g Sr-ferrite powders that had been suspended in 50-mL aqueous solution containing the surface active agent APS. To improve the contacts between ferrites and anilines in aqueous solution, Sr-ferrite powder was dispersed in deionized water by ultrasonic waves with an oscillation frequency of 42 kHz for 30 min before polymerization. The monomer solution for polymerization was created by mixing aniline and HCl in 100-mL deionized water. The molar ratio of aniline to HCl in solution was 1:3 and the concentration of aniline in solution was 0.033 M. The required amount of aniline aqueous solution was added drop by drop to each flask containing the suspended Sr-ferrite solution; the polymerization was allowed to proceed at temperature between 0 and 5 °C under mechanical stirring for 3 h. After the solid core–shell particles were formed, the solid products were collected and washed with methanol and deionized with water several times sequentially. Finally, the products were dried in a vacuum oven at 100 °C for 24 h.

Characterization

The XRD patterns of the samples were collected using powder X-ray diffraction (XRD) (Siemens D5000X) with Cu Kα radiation ($\lambda = 0.15418$ nm). Fourier transmission infrared (FTIR) spectra were recorded on a TENSOR 27 spectrometer (Varian) in the range of 400–4000 cm^{-1} using KBr pellets. Thermogravimetric analysis (TGA, PERKIN-ELMER) was used to measure the thermal decomposition behavior of the 1200 °C $Sr(MnTi)_xFe_{12-2x}O_{19}$/PANI powders. The heating rate was 10 °C/min, and the flow rate of air in the thermal property measurements was 10 mL/min. The morphology was characterized by a JSM-6390 scanning electron microscope (SEM) and JEOL2000-EX 2 transmission electron microscope (TEM). Magnetic measurements were carried out at room temperature using a vibrating sample magnetometer (VSM, Lake Shore, model 7400) with a maximum magnetic field of 15 kG. The specimens for microwave adsorption testing were prepared by homogeneously mixing the 60 wt% composite powders with 40 wt% thermal plastic resin (TPR), utilizing a high-heat machine (Molding Test Press Tester 0–150 kg/cm^2, 0–400 °C, HT-8122B) to manufacture microwave absorption-films (155 mm × 155 mm × 2.0 mm) at temperatures of approximately 150–175 °C (stress design 10–30 kg/cm^2, 15 min). A high-frequency network analyzer (Vector Network Analyzer HP8722ES) was used to measure the reflection loss (RL) of electromagnetic radiation of the polyaniline–TPR, $Sr(MnTi)_xFe_{12-2x}O_{19}$–TPR, $Sr(MnTi)_xFe_{12-2x}O_{19}$/PANI–TPR composite materials. The RL curves were calculated from the complex relative permeability and permittivity at a given frequency and absorber thickness with the following equations:

$$Z_{in} = \sqrt{\frac{\mu_\gamma}{\varepsilon_\gamma}} \tan h\left[\left(j\frac{2\pi}{\lambda}\right) d\sqrt{\mu_\gamma \varepsilon_\gamma}\right] \quad (3)$$

$$\Gamma = \frac{Z_{in} - 1}{Z_{in} + 1} \quad (4)$$

$$RL(dB) = 20 \times \log|\Gamma| \quad (5)$$

where λ is the frequency, d is the thickness of the absorber, j is the condition of vacuum, ε_γ and μ_γ are the relative complex permeability and permittivity, respectively, of the absorber medium, Γ is the reflection parameter, Z_0 the impedance of air, and Z_{in} is the input impedance of the absorber [37].

Results and discussions

X-ray powder diffraction

The XRD patterns of $Sr(MnTi)_xFe_{12-2x}O_{19}$ and $Sr(MnTi)_xFe_{12-2x}O_{19}$/PANI composite nanoparticles and PANI are shown in Fig. 1. As shown in Fig. 1b and d, respectively, the crystal structures of $Sr(MnTi)_{1.5}Fe_{8.0}O_{19}$ and $Sr(MnTi)Fe_{10}O_{19}$ annealed at 1200 °C for 2 h were determined by the powder X-ray diffraction technique. The X-ray diffraction patterns of $Sr(MnTi)Fe_{10}O_{19}$ particles present the M-type structure, and the XRD spectra showed the diffraction peaks similar to hexagonal $SrFe_{12}O_{19}$ (110), (107), (114), (203), (205), (206), (0014), (304), (221), and (404), which were all observed in each curve [38]. The lattice constant a of $Sr(MnTi)Fe_{10}O_{19}$ is 5.88–5.90 Å. A typical XRD pattern of polyaniline shows one broad

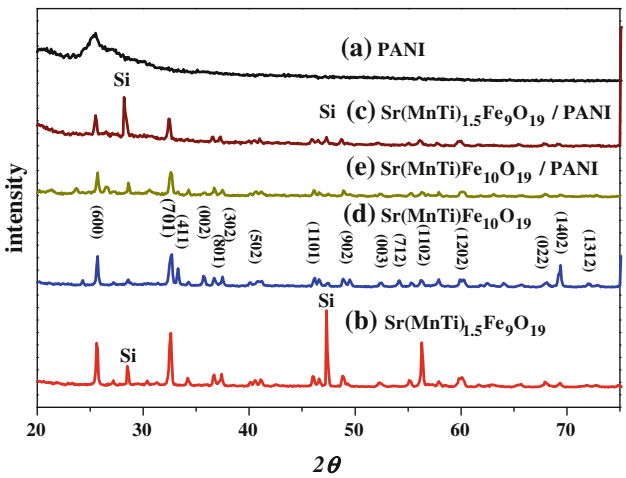

Fig. 1 XRD patterns of (*a*) PANI, (*b*) $Sr(MnTi)_{1.5}Fe_9O_{19}$ particles, (*c*) $Sr(MnTi)_{1.5}Fe_9O_{19}$/PANI composite, (*d*) $Sr(MnTi)Fe_{10}O_{19}$, and (*e*) $Sr(MnTi)Fe_{10}O_{19}$/PANI composite

diffraction peak centered at $2\theta = 25.51°$ (see Fig. 1a), which can be ascribed to the periodicity parallel and is perpendicular to the polymer chains [39]. Figure 1c and e shows the values of the $Sr(MnTi)_xFe_{12-2x}O_{19}$/PANI composite, which contains the characteristic peaks of PANI and $Sr(MnTi)_xFe_{12-2x}O_{19}$ ($x = 1.0, 1.5$), including the peaks at $2\theta = 25.62°$, 32.52°, 33.43°, 35.72°, 36.76°, 37.57°, 40.88°, 46.04°, 48.91°, 52.35°, 56.25°, 60.15°, 68.29°, 69.33°, 72.08°, and 74.48°. These results indicated that the structure of the core materials is a hexagonal structure, and the $Sr(MnTi)_xFe_{12-2x}O_{19}$/PANI core–shell composites were obtained.

FTIR spectral analysis

The FTIR spectra of the $Sr(MnTi)Fe_{10}O_{19}$, $Sr(MnTi)Fe_{10}O_{19}$/PANI composites and PANI sample without $Sr(MnTi)Fe_{10}O_{19}$ core-particles under the same conditions are shown in Fig. 2. It is observed in Fig. 2c that there is a peak at 1388 and 1647 cm^{-1}, corresponding to vibrations of $Sr(MnTi)Fe_{10}O_{19}$ in each curve. The characteristic peaks of PANI occur at 1110, 1237, 1291, 1486, 1565, and 805 cm^{-1}. The peaks at 1565 and 1486 cm^{-1} are attributed to the characteristic C=C stretching of the quinoid and benzenoid rings, and the peaks at 1291 and 1237 cm^{-1} correspond to N–H bending and asymmetric C–N stretching modes of the benzenoid ring, which were also observed in each curve of Fig. 2b. The peak near 1110 cm^{-1} is associated with vibrational modes of N=Q=N (Q refers to the quinonic-type rings), indicating that PANI was formed in our sample. The peak at 805 cm^{-1} is attributed to the out-of-plane deformation vibration of the *p*-disubstituted benzene ring.

The absorption peaks of the $Sr(MnTi)Fe_{10}O_{19}$/PANI composite shifted to 1119, 1298, 1396, and 1475 cm^{-1} (see Fig. 2a). The absorption peak of the composite with $Sr(MnTi)Fe_{10}O_{19}$/PANI is approximately 8 cm^{-1} shifted, compared to that of the pure PANI. These results indicate the good quality of the coating of $Sr(MnTi)Fe_{10}O_{19}$ particle with PANI in the composite.

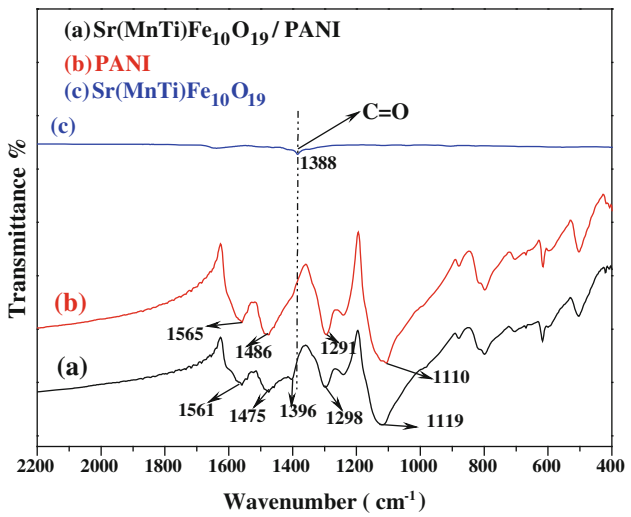

Fig. 2 FT-IR spectra prepared with different (*a*) $Sr(MnTi)Fe_{10}O_{19}$/PANI composite, (*b*) PANI, and (*c*) $Sr(MnTi)Fe_{10}O_{19}$

Thermogravimetric analysis measurements

TGA curves of the $Sr(MnTi)_xFe_{12-2x}O_{19}$ ($x = 1.0, 1.5, 2.0$) dry sol–gels (Fig. 3) show that there are two steps of primary weight loss, which occur at temperature between 150–250 °C and 250–350 °C. A weight loss in the first step of approximately 20–25% was considered to be due to the oxidation reduction of NO_3^- ions and the free glycine molecules that did not link to the metal ions. Approximately 25–30% of weight loss in the second step corresponded to the decomposition reactions or oxidation–reduction reactions of the nitrate ions and liganded glycine molecules. Approximately 2–5% of weight loss occurred at temperature between 350 and 600°C. The third step of weight loss was considered to be the oxidation reaction of the residual carbon atoms in the surface of the ashes.

The TGA curve of $Sr(MnTi)_xFe_{12-2x}O_{19}$ ($x = 1.0, 1.5, 2.0$), annealed at 1200 °C, and PANI composites in Fig. 4a shows 100% PANI. Approximately 10% weight loss occurred at temperatures between 0 and 150 °C, which was due to vaporization of water in polyaniline. Figure 4a also indicates that pure PANI material will undergo a redox reaction or decomposition initially at around 150 °C. PANI has the greatest weight loss (~96.7%) at temperatures between 250 and 600 °C. Figure 4b–d shows that the starting decomposition temperature of PANI depends on the amount of $Sr(MnTi)_xFe_{12-2x}O_{19}$, which is the shell material of the core–shell hexagonal ferrites. In the $Sr(MnTi)_xFe_{12-2x}O_{19}$ ($x = 1.0, 1.5, 2.0$) and PANI core–shell structure composites approximately 71.1–26.5%

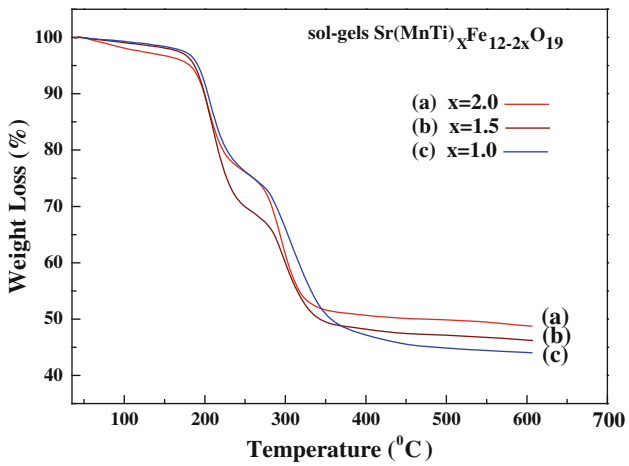

Fig. 3 TGA curves of the dry $Sr(MnTi)_xFe_{12-2x}O_{19}$ sol–gels

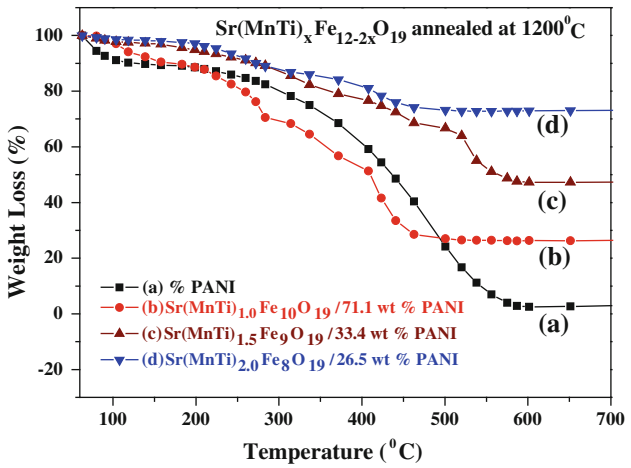

Fig. 4 TGA curves of $Sr(MnTi)_xFe_{12-2x}O_{19}$/PANI. (*a*) 100% PANI, (*b*) $Sr(MnTi)_{1.0}Fe_{10}O_{19}$/71.1 wt% PANI, (*c*) $Sr(MnTi)_{1.5}Fe_9O_{19}$/33.4 wt% PANI, and (*d*) $Sr(MnTi)_{2.0}Fe_8O_{19}$/26.5 wt% PANI

PANI materials of weight loss occurs at a temperature between 350 and 500 °C. This variation in initial decomposition temperature occurs because the more the hexagonal ferrite, the stronger the strontium manganese titanium hexaferrites/polyaniline composites' structure. It is obvious that the more strontium manganese titanium hexaferrites/PANI hybrid, the more remnant weight percent there is after decomposition at 600 °C.

SEM and TEM observations

The SEM micrograph diameter of the hexagonal $Sr(MnTi)Fe_{10}O_{19}$ powders were found to increase, distributed in the range of 50–250 nm (Fig. 5a) after heat treatment at 1200 °C for 2 h. Figure 5b shows the SEM image of the core–shell $Sr(MnTi)Fe_{10}O_{19}$/PANI composites. The image indicates that the core–shell are coated by polyaniline and form spherical coral-like particles, which have diameters around 100–500 nm and are connected by the polymer. To investigate the detailed structure of $Sr(MnTi)Fe_{10}O_{19}$/PANI core–shell samples, TEM was performed. The $Sr(MnTi)Fe_{10}O_{19}$/PANI powder composites were dissolved with *N*-methyl-2-pyrrolidone (NMP), which is a good dissociation solvent for PANI. Figure 5c shows the $Sr(MnTi)Fe_{10}O_{19}$ particles coated by the PANI layer and indicates that the $Sr(MnTi)Fe_{10}O_{19}$ particles are imbedded in the PANI matrix. The black region shows the $Sr(MnTi)Fe_{10}O_{19}$ particles, and the gray colored shell is PANI in the composite, due to the different electron penetrability.

Magnetic properties

The magnetic hysteresis loop measurements of $Sr(MnTi)_xFe_{12-2x}O_{19}$ annealed at 1200 °C are shown in Fig. 6, along

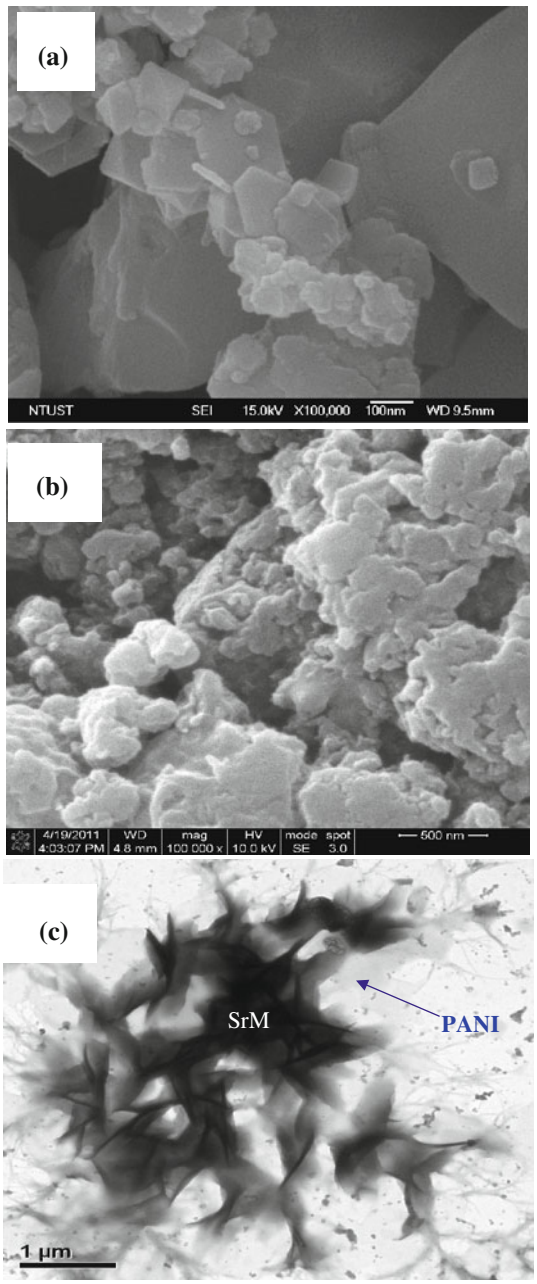

Fig. 5 SEM images of **a** $Sr(MnTi)Fe_{10}O_{19}$ particles, **b** $Sr(MnTi)Fe_{10}O_{19}$/PANI composites. TEM images of **c** $Sr(MnTi)Fe_{10}O_{19}$/PANI composite

with the area of the magnetic hysteresis loop of the powder $Sr(MnTi)Fe_{10}O_{19}$ (Fig. 6a). The saturation magnetization (M_s), remanence magnetization (M_r), and coercivity (H_c) of this specimen are 12.06 emu/g, 0.81 emu/g, and 0.805 kG, respectively. Figure 6b–d shows the hysteresis loops of the $Sr(MnTi)_{1.5}Fe_{9.0}O_{19}$ as well as $Sr(MnTi)Fe_{10}O_{19}$/PANI, $Sr(MnTi)_{1.5}Fe_{9.0}O_{19}$/PANI composites, and the pure PANI at room temperature. It is observed that the saturation magnetization (M_s), coercivity (H_c), and remanence magnetization (M_r) values for $Sr(MnTi)_{1.5}Fe_{9.0}O_{19}$ and PANI

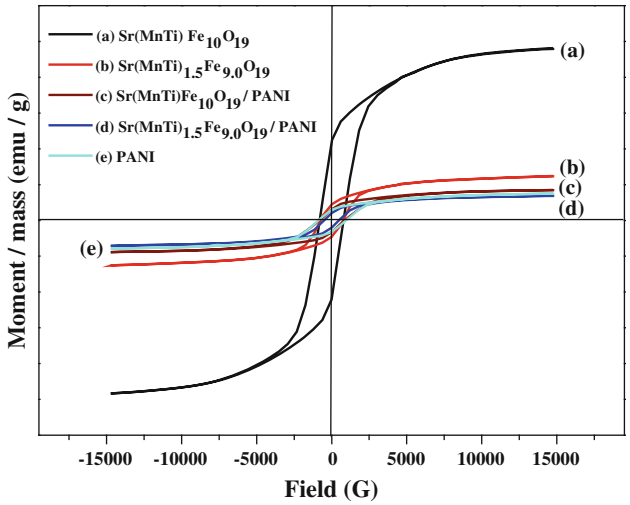

Fig. 6 Hysteresis loops of (*a*) $Sr(MnTi)Fe_{10}O_{19}$ particles, (*b*) $Sr(MnTi)_{1.5}Fe_{9.0}O_{19}$ particles, (*c*) $Sr(MnTi)Fe_{10}O_{19}$/PANI, (*d*) $Sr(MnTi)_{1.5}Fe_{9.0}O_{19}$/PANI composite, and (*e*) PANI

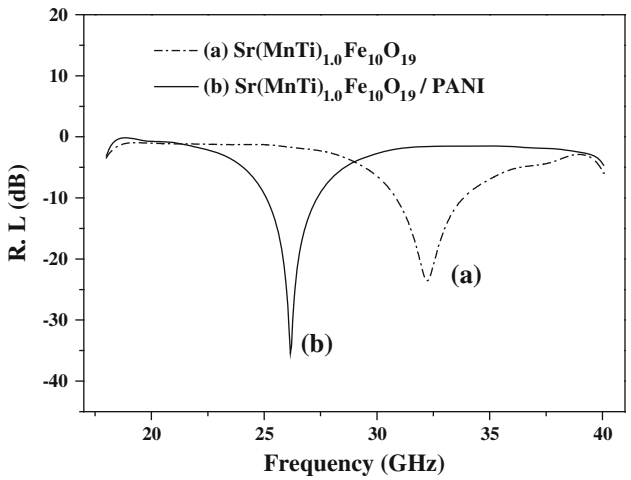

Fig. 7 The microwave absorption RL of (*a*) $Sr(MnTi)_{1.0}Fe_{10}O_{19}$ and (*b*) $Sr(MnTi)_{1.0}Fe_{10}O_{19}$/PANI composites

are $M_S = 2.16$, 3.12 emu/g, $H_c = 0.086$, 0.75 kG, and $M_r = 0.81$, 1.12 emu/g (Fig. 6b, e). In contrast, the $Sr(MnTi)Fe_{10}O_{19}$/PANI and $Sr(MnTi)_{1.5}Fe_{9.0}O_{19}$/PANI composites under an applied magnetic field exhibit a clear hysteretic behavior. As seen in Fig. 6c and d, the $M_S = 1.92$, 1.74 emu/g, and $H_c = 0.92$, 0.51 kG are lower than those of pure $Sr(MnTi)_xFe_{12-2x}O_{19}$ particles. When pure $Sr(MnTi)Fe_{10}O_{19}$ particles were coated with PANI (Fig. 6d), the values of M_s, H_c, and M_r all decreased with increasing PANI values, and contraction of the hysteresis loop area is seen. These results show that the pure $Sr(MnTi)Fe_{10}O_{19}$ particle cores are responsible for the magnetic behavior of the pure $Sr(MnTi)Fe_{10}O_{19}$/PANI composites. According to the equation $M_s = \varphi m_S$, M_s is related to the volume fraction of the particles (φ) and the saturation moment of a single particle (m_S) [40]. It can be assumed that the M_s of the $Sr(MnTi)_xFe_{12-2x}O_{19}$/PANI composite depends mainly on the volume fraction of the magnetic hexaferrite particles, due to the contribution of the non-magnetic PANI coating layer to the total magnetization, resulting in a decrease in the saturation magnetization. The magnetic properties observed for magnetic particles are a combination of many anisotropy mechanisms. An effective anisotropy constant (K) could be obtained by adding the bulk anisotropy and surface contributions, and the following expression has been used to account for K [41]:

$$K = K_b + (6/d)K_S \quad (6)$$

where K_b is the bulk magnetocrystalline anisotropy, K_S is the surface anisotropy, and d is the particle diameter. K_S is usually the maximum for free surfaces and is reduced by solid coverage. The decrease in K_S resulting from the particle coverage by the PANI reduces the effective magnetocrystalline anisotropy (K) and therefore decreases H_c.

Microwave absorption

A high-frequency network analyzer (Vector Network Analyzer HP8722ES) was used to examine the reflectivities of the pure ferrites and the core–shell ferrites. Figure 7 and Table 1 show the characteristic absorption of materials at frequencies between 18.0 and 40.0 GHz. It was found that the conductivity of PANI coated on the Sr-M dramatically affects the microwave absorption of the materials. Composite specimens comprising the PANI, $Sr(MnTi)_xFe_{12-2x}O_{19}$, core–shell $Sr(MnTi)_xFe_{12-2x}O_{19}$/PANI materials, and a TPR demonstrated a microwave absorbing band-wide between 26.0 and 38.0 GHz, where reflections observed on a network analyzer lost −15.7 to −35.5 dB.

Conclusion

A $Sr(MnTi)_xFe_{12-2x}O_{19}$/PANI core–shell composite was successfully synthesized by the facile oxidative chemical

Table 1 Microwave absorption of $Sr(MnTi)_xFe_{12-2x}O_{19}$/PANI composites

Samples	Frequency (GHz)	Reflection (dB)	Thickness (mm)
$Sr(MnTi)_{1.0}Fe_{10}O_{19}$	32.21	−23.5	2.0
$Sr(MnTi)_{1.5}Fe_{9.0}O_{19}$	26.65	−15.7	2.0
$Sr(MnTi)_{2.0}Fe_{8.0}O_{19}$	28.08	−15.9	2.0
$Sr(MnTi)_{1.0}Fe_{10}O_{19}$/PANI	26.17	−35.5	2.0
$Sr(MnTi)_{1.5}Fe_{9.0}O_{19}$/PANI	37.94	−17.8	2.0
$Sr(MnTi)_{2.0}Fe_{8.0}O_{19}$/PANI	32.50	−31.5	2.0

polymerization of aniline in the presence of $Sr(MnTi)_xFe_{12-2x}O_{19}$ ($x = 0$, 1.0, 1.5, 2.0) particles. The core–shell structure of the $Sr(MnTi)_xFe_{12-2x}O_{19}$/PANI composite was characterized by XRD, FT-IR, TGA, SEM, and TEM. The intrinsic magnetic hysteresis loop measurements revealed that the M_s and H_c decreased with the polyaniline content. The core–shell $Sr(MnTi)_xFe_{12-2x}O_{19}$/PANI–TPR materials have stronger absorption for microwave between 18.0 and 40.0 GHz than pure hexagonal ferrite, $Sr(MnTi)_xFe_{12-2x}O_{19}$–TPR. A nearly 40% band-width range of RL peaks below −20 dB at frequencies between 25.0 and 37.8 GHz was observed in the core–shell $Sr(MnTi)_xFe_{12-2x}O_{19}$/PANI–TPR composite. Improvement in the adsorption performance may be attributed to the relative permittivity change induced by the exchange coupling interaction between the conducting polymer and the magnetic materials.

Acknowledgement The authors would like to thank the National Science Council of the Republic of China, Taiwan, for financially supporting this research under Contract No. NSC 99-2218-E-145-006.

References

1. Robison TM (1990) Mater Res Bull 25:1401
2. Qiu J, Liang L, Gu M (2005) Mater Sci Eng A 393:361
3. Somogyvari Z, Svaib E, Meszaros G, Krezhov K, Konstantinov P, Nedkov I, Bouree F (2002) J Appl Phys 91(9):6185
4. Meshram MR, Sinha B, Agrawal NK, Misra PS (2002) IEEE Antennas Propag Soc Int Symp 2:790
5. Barb D, Diamandescu L, Rusi A (1986) J Mater Sci 21:1118. doi:10.1007/BF00553240
6. Wang ML, Shih ZW (1991) J Cryst Growth 114:435
7. Kubo O, Ido T, Yokoyama H (1982) IEEE Trans Magn 18:1122
8. Kuo PC, Yao YD, Tzang WI (1993) J Appl Phys 73:10
9. Pankov VV, Pernet M, Germi P, Mollard P (1993) J Magn Magn Mater 120:69
10. Jacobo SE, Blesa MA, Domingo-Pascual C, Rodpigguez-Clemente R (1997) J Mater Sci 32:1025. doi:10.1023/A:1018582423406
11. Zheng Z, Guo B, Mei X (1989) J Magn Magn Mater 78:73
12. González-Carreño T, Morales MP, Serna CJ (2000) Mater Lett 43:97
13. Zhong W, Ding WP, Zhang N, Hong JM, Yan QJ, Du YW (1997) J Magn Magn Mater 168:196
14. Srivastava A, Singh P, Gupta MP (1987) J Mater Sci 22:1489. doi:10.1007/BF01233152
15. Roos W (1980) J Am Ceram Soc 63:601
16. Lin CS, Huang CC, Huang TH, Wang GP, Peng CH (2007) Mater Sci Eng B 139:24
17. Lucchini E, Meriani S, Slokar G (1983) J Mater Sci 18:1331. doi:10.1007/BF01111950
18. Shirk BT, Buessem WR (1970) J Am Ceram Soc 53:192
19. Huang J, Zhuang H, Li WL (2003) Mater Res Bull 38:149
20. Manoharam SS, Patio KC (1993) J Solid State Chem 102:267
21. Chakraborty A, Devi PS, Maiti HS (1995) J Mater Res 10(4):918
22. Bhaduri S, Bhaduri SB, Zhou E (1998) J Mater Res 13:156
23. Sekar MMA, Halliyal A (1998) J Am Ceram Soc 81:380
24. Mukasyan AS, Costello C, Sherlock KP, Lafarga D, Varma A (2001) Sep Purif Technol 25:117
25. Mäkelä T, Pienimaa S, Taka T, Jussila S, Isotalo H (1997) Synth Met 85:1335
26. Kuwabata S, Masui S, Yoneyama H (1999) Electrochim Acta 44:4593
27. Kan JQ, Pan XH, Chen C (2004) Biosens Bioelectron 19:1635
28. Ahmad N, MacDiarmid AG (1996) Synth Met 78:103
29. Rose TL, Antonio SD, Jillson MH, Kron AB, Suresh R, Wang F (1997) Synth Met 85:1439
30. Yavuz O, Ram MK, Aldissi M, Poddar P, Hariharan D (2005) J Mater Chem 15:810
31. Zhang YY, Liu JL, Zhu YX, Shang Y, Yu M, Huang X (2009) J Mater Sci 44:3364. doi:10.1007/s10853-009-3439-2
32. Lee SP, Chen YJ, Ho CM, Chang CP, Hong YS (2007) Mater Sci Eng B 143:1
33. Ding H, Liu XM, Wan M, Fu SY (2008) J Phys Chem B 112:9289
34. Jiang J, Li L, Xu F (2007) J Phys Chem Solids 68:1656
35. Yuan CL, Hong YS (2010) J Mater Sci 45:3470. doi:10.1007/s10853-010-4375-x
36. Yuan CL, Hong YS, Lin CH (2011) J Magn Magn Mater 323:1851
37. Huo J, Wang L, Yu H (2009) J Mater Sci 44:3917. doi:10.1007/s10853-009-3561-1
38. Gorter EW (1950) Nature (London) 165:798
39. Sauzedde F, Elaissari A, Pichot C (1999) Colloid Polym Sci 277:846
40. Battle X, Labarta A (2002) J Phys D 35:15
41. Jiang J, Ai LH, Qin DB, Liu H, Li LC (2009) Synth Met 159:695